INTERNATIONAL JOURNAL FOR NUMERICAL AND ANALYTICAL METHODS IN GEOMECHANICS
*Int. J. Numer. Anal. Meth. Geomech.*, **23**, 1609–1629 (1999)

# DETERMINATION OF PERMEABILITY OF SOILS USING THE MULTIPLE PIEZO-ELEMENT PENETROMETER

CHUNG R. SONG[†], GEORGE Z. VOYIADJIS*[,‡] AND MEHMET T. TUMAY[§]

*Department of Civil and Environmental Engineering, Louisiana State University, Baton Rouge, LA 70803, U.S.A.*

## SUMMARY

The current method of determining the hydraulic properties of soils using piezocone penetration test (PCPT) requires the advancement of the piezocone penetrometer to the desired depth and holding (or arresting) it for the dissipation test. In order to obtain the hydraulic properties, one analyses the pore water dissipation test results by two-dimensional or three-dimensional radial drainage consolidation. This conventional procedure is methodologically simple and presents relatively reliable values of permeability compared to other field test methods. However, it is still challenging for field engineers and needs to be improved.

The piezocone penetrometer intrudes into the ground with the speed of 2 cm/s. Thus, the test mechanism is a kind of strain-controlled condition with partial drainage. Therefore, the excess pore pressure during the piezocone penetration is a function of the permeability of the soil as well as the stress–strain parameters. Thus, with the proper coupled theory of mixtures which can take into account the coupling of solid and pore water flow, one can predict the permeability of the soil from the pore pressure response during PCPT.

In this study, the coupled theory of mixtures of the soil grains and the pore water is used in order to predict the permeability of the soil from the excess pore pressure generated from the multiple piezo-element PCPT 'on the fly'. An elasto-plastic, finite strain constitutive equation in an updated Lagrangian reference frame is used in this work. Using the proposed method, a reliable value of the permeability of soil is obtained conveniently without the use of the pore pressure dissipation tests. Copyright © 1999 John Wiley & Sons, Ltd

KEY WORDS: permeability; piezocone; coupled theory of mixtures; elasto-plastic finite strain; updated Lagrangian reference frame; pore water pressure

* Correspondence to: George Z. Voyiadjis, Department of Civil and Environmental Engineering, College of Engineering, Louisiana State University, Baton Rouge, LA 70803-6405, U.S.A. E-mail: cegzv1@unixl.sncc.lsu.edu
[†] Doctoral Candidate
[‡] Boyd Professor
[§] Professor and Associate Dean for Research

CCC 0363–9061/99/131609–2117.50

*Received November 1998*
*Revised 22 February 1999*

## 1. INTRODUCTION

A somewhat crude type of the penetrometer was introduced as early as the Roman era. The number of slaves required to push a certain rod into the ground was used to quantify the strength of the ground. With the advent of modern science, this method was refined and diversified to several kinds of penetrometers, such as the cone penetrometer, the standard penetrometer, the Swedish penetrometer, etc. Among these penetrometers, the cone penetrometer is acknowledged as one of the most widely used ground probing devices due to its superior performance (repeatability, convenience, economics, etc.).

A modern type of cone penetrometer was first introduced in early 20th century in European countries, and it was called the mechanical cone penetrometer.[1] The mechanical cone penetrometer measured the tip resistance by utilizing a manual driving system (chain + gear system) and a mechanical force measuring system (probing rings or mechanical pressure gages). Later the cone penetrometer evolved that could measure both the tip and friction resistance was appeared, and it was called the mantle cone penetrometer. These mechanical cone penetrometers were not equipped with the modern sensors and automatic driving systems. However, they presented consistent and reliable results with less cost compared to Standard Penetration Test (SPT). Traditional mechanical cone penetrometers use the double rod system — inner rods and outer rods. The test is carried out by pushing the inner rods for measurements, and subsequently by pushing the outer rods for the advancement of the whole system. Thus, the test procedure is a stop and go process; it is not continuous.

With the aid of the modern sensors and electric technology, the electronic cone penetrometer was first introduced in 1970s.[2] It provided greatly increased productivity and overall performance. The electronic cone penetrometer utilized the electronic measuring system (load cell) and motorized driving system instead of the mechanical measuring system and the manual driving system; thus, the reading could be done automatically by electronic readout without stopping the penetration. This also allowed the penetration speed to be controlled more accurately.

The piezocone is a type of electronic cone penetrometer, which has the pore pressure monitoring capability to enhance the assessment of engineering parameters, especially the hydraulic properties of the soils. Measurement of the pore water pressure generated while advancing a cone tip into the ground, and its subsequent dissipation when the penetration is stopped was first made in Sweden in the early 1970s.[2,3] Earlier version of the piezocone penetrometer did not have the capability of simultaneous measurement of the cone resistance (tip resistance and/or side friction) and the pore pressure. Subsequent developments in transducer technology during the early 1980s involved the incorporation of piezometric elements into the electronic cone penetrometers. This made it possible to measure the pore pressures, cone resistance and skin friction simultaneously. Tumay *et al.*[4] is known as the first group who utilized the simultaneous measurement of cone resistance, frictional resistance and pore pressure at multiple locations.[5] Many researchers contributed to the application of the simultaneous measurement of the cone resistance and pore pressure,[1,5–10] and opened the era for the fully equipped piezocone penetrometer.

Currently, several sensors can be attatched to the cone probe at the same time in order to obtain the various soil properties. Accelerometers can be attached to detect the seismic response of soils.[11] Electric resistivity sensors, thermal sensors or infrared sensors can be attached to detect the ground contamination. A microphone may be also attached to detect the sonic response of ground, while the radioactive sensors can be attatched to detect the radioactive materials in the ground.[1,8] Virtually any kind of sensors can be incorporated with the modern cone

 

penetrometers. For geotechnical purposes, the most widely used combination is the two load cells for the tip resistance and the side friction, one piezometer for the pore pressure response, and one inclination sensor for the depth correction.

All of these sensors are electronic sensors, and the industrial computer-based electronic readouts are used, thus most of the measured response is recorded and analysed with real-time basis during the penetration process. In fact, many of the modern piezocone manufacturers also supply the real-time measuring readout and analysis software. However, the permeability is not determined directly during the penetration process, because it needs the extra test termed the dissipation test. This extra process decreases the major drawback of the efficiency of the PCPT.

Recently, there are several efforts to increase the efficiency of the PCPT even further by mechanical improvement. Tumay[12] developed the spiral rod for continuous advancement of the cone tip, which does not require the connection of the pushing rod. Environmental mechanics AB[13] developed the wireless piezocone penetrometer called *memocone*, which removed the hassle of wiring during PCPT. Mayne and Rix[14] combined the pressuremeter and cone penetrometer for the simultaneous tests of pressuremeter and cone penetrometer.

Recently, Voyiadjis and Song[15] predicted the permeability of soils utilizing the coupled theory of mixtures and the pore pressures at the cone tip generated during PCPT. This study, along with the pioneering study of Voyiadjis and Song,[15] by removing the necessity of the dissipation test, brings a fundamental improvement in the PCPT applications in addition to the aforementioned mechanical improvements presented here.

## 2. EVALUATION OF CONVENTIONAL METHODS

Along with the significant evolution of the mechanical aspects of the PCPT, there are also, great achievements in the analysis method of the PCPT. However, many of these achievements are concentrated on the real-time measurement and the interpretation of the stress–strain properties of soils. From the view of the utilization of the penetration pore pressure response, most of the efforts are focused on the correction of the tip resistance and side friction, or the soil classification purpose. Relatively fewer efforts are focused on the interpretation of the penetration pore pressure response itself. In fact, many of these theories aim at the analysis of the pore pressure dissipation data, and not at analysing the penetration pore pressure directly. Thus, in spite of the highly modernized and speedy nature of the PCPT, the determination of the permeability is not adequately modernized and is not speedy enough. This may be partly due to the fact that the usage of the PCPT is mostly focussed on obtaining the stress–strain behaviour of soils. It is also partly due to the fact that the initial research on permeability started with a rather simple method — the so-called dissipation test (or holding test) method. The dissipation test method utilizes the pore pressure dissipation test results, which are obtained during the holding (or arresting) period of the piezocone. Even today, many research projects are conducted using this method. However, this method has two major explicit drawbacks as follows:

a. Required time for the dissipation test is long: Typically, without the dissipation test, the whole procedure for one PCPT takes one and half to two hours for 30 m of penetration. With the dissipation test, it takes about an additional one hour for a single point of permeability data. Thus, the dissipation test largely decreases the efficiency of the PCPT.
b. Continuous permeability profile is impossible: Because of the prolonged required time for the dissipation test, only a limited number of dissipation tests can be carried out. Thus, continuous

 

permeability profiles cannot be obtained, even though other profiles (tip resistance, friction resistance, generated pore pressure, etc.) are practically continuous.

In addition to the aforementioned explicit drawbacks, the conventional method has the following implicit drawbacks. Conventionally, the pore pressure dissipation test results are used for the determination of the permeability (or coefficient of consolidation.). The pore pressure dissipation test assumes a certain dissipation pattern (like a cylindrical heat sink in a homogeneous media in some ideal boundary conditions). Thus, the conventional method inherently has some limitations depending on the real soil conditions. The limitation of the conventional method is discussed below.

The partial differential equations, boundary conditions and initial conditions for the conventional method are, respectively:

*Partial differential equation*:

$$\partial\sigma'/\partial t = (\partial\sigma/\partial t) - (\partial u/\partial t) = c_{\mathrm{h}}[(\partial^2 u/\partial r^2) + (1/R)(\partial u/\partial r)] + c_z\left[\frac{\partial^2 u}{\partial z^2}\right] \tag{1}$$

*Boundary conditions*:

$$u = 0 \text{ at } r = \infty,\ z = \infty, \text{ and } z = -\infty$$

$$u' = k \text{ at } r = R,\ z = 0$$

*Initial condition*:

$F = g$ (stress strain functions such as those obtained from the cavity expansion theory)

In equation (1), $\sigma'$ is the effective stress, $\sigma$ is the total stress, $u$ is the excess pore pressure, $t$ is the elapsed time, $c_{\mathrm{h}}$ is the horizontal consolidation coefficient, $c_z$ is the vertical consolidation coefficient, $R$ is the radius of the cone, $r$ is the radial axis, and $z$ is the vertical axis of the cylindrical coordinate system. The solution of equation (1) is not straightforward. It can be solved using a special numerical technique such as the Crank–Nicholson technique. Torstensson[2,16] simplified equation (1) by assuming negligible vertical drainage (assume the effect of $c_z$ and related term is minor) and a constant total stress (assume $(\partial\sigma/\partial t) = 0$). Torstensson[2,16] presented a convenient graphical solution, which is similar to that of Terzaghi's[17] one-dimensional consolidation solution. However, inaccurate results can also result if the field conditions are not close to the assumptions given above. Gupta and Davidson,[18] used equation (1) instead of Torstensson's simplified version[2,16] with the assumed boundary conditions (since equation (1) cannot be solved with boundary conditions such as $u = 0$ at $r = \infty$.). Although Gupta and Davidson[18] obtained better results, however, the fundamental drawbacks of equation (1) and its simplified version by Torstensson[2,16] are not eliminated.

Essentially, the pore pressure response from the PCPT should follow the curves shown in Figure 1. Figure 1 shows a conceptual and slightly exaggerated excess pore pressure response of the soil element, which is located at the projected centreline of the piezocone penetration route. Initially, the location of the piezocone tip is far above this soil element, and there is no excess pore pressure. This means that the soil element is very far from the cone tip and is not affected by the piezocone penetration. As the time progresses, the penetrating cone tip comes closer to the soil element, and the stress bulb of the penetrating cone tip gradually starts to distribute the stress on this soil element. This will result in the gradual increase of the excess pore water pressure (may or may not be linearly changing). As the penetrating cone tip passes through this soil element, the

 

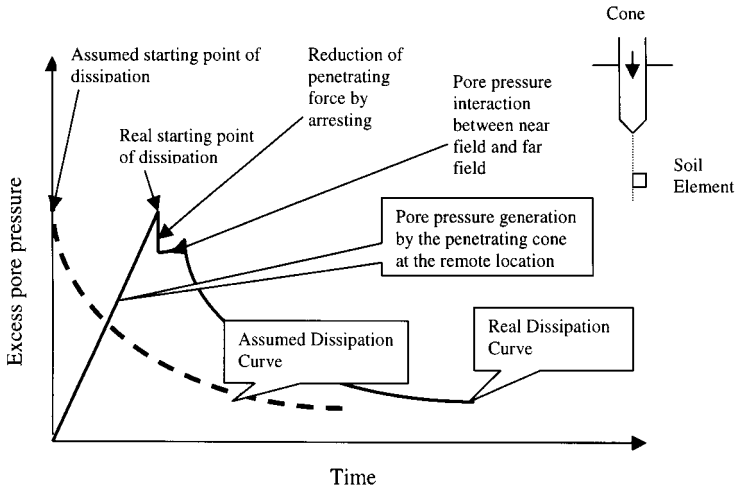


Figure 1. Conceptual shape of pore pressure response for a soil element during the penetration of piezocone penetration

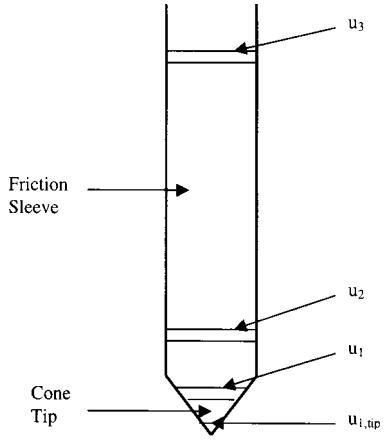


Figure 2. Typical locations of piezo–elements for piezocone penetrometer

maximum disturbance occurs and the maximum excess pore pressure takes place (for normally consolidated soils). When the penetrating cone tip stops at this soil element location, there will be an immediate drop of the excess pore pressure due to the reduced axial force. At the same time, the interaction of pore pressure between the near and far field takes place, and results in the small increase or decrease of the pore pressure.[19,20] As observed previously by Voyiadjis and Abu-Farsakh,[21] the pore pressure during penetration is maximum at the cone face (typically known as $u_1$ position). Thus, if one has the porous element at the cone tip location (typically known as $u_{1,\text{tip}}$) or $u_2$ position, a small increase of pore pressure will be expected because of the pore water inflow from the $u_1$ position (See Figure 2, for $u_{1,\text{tip}}$, $u_1$, $u_2$, and $u_3$ location). If one has the porous element at the $u_1$ element location, this change of pore pressure will be very small, and may not be

 

distinguishable. This explanation is for the normally consolidated soils. For the over consolidated soils, similar behaviour can be predicted if the dilation phenomenon is considered.

Considering the aforementioned factors, one can find that the dissipation test in the piezocone penetrometer is carried out with an unstable background pore pressure condition. This is due to the incorrect magnitude of the initial pore water pressure, the initial time of dissipation, and the pore water pressure interaction. However, the assumed dissipation curve is based on the ideally stable background pore pressure condition.

Clearly, a more reasonable method that does not have the aforementioned drawbacks is needed. However, the behaviour of the soil around the penetrating cone tip is very complex in nature because of the geometrical shape of the cone tip, large strains, drainage conditions, etc. Attempts have been made in recent years to develop analytical models for simulating the complex problem of the cone penetration process. Advanced one-dimensional consolidation theories incorporating the finite strain, change of the permeability and compressibility characteristics are developed by Gibson *et al.*,[22,23] and Schiffman.[24] Carter *et al.*[25,26] and Prevost[27,28] extended these theories to incorporate the elasto-plastic soil behaviour and the finite strains in 3D consolidation. Prevost[27] developed a general theory for porous media based on the concepts of the coupled theory of mixtures. Kiousis and Voyiadjis[29] modified for a Lagrangian reference frame. Voyiadjis and Abu-Farsakh[21] and Abu-Farsakh *et al.*[30] used the coupled theory of mixtures and large strain constitutive equations in order to numerically simulate the cone penetration tests in clayey soils. In the relatively early theories (Carter *et al.* and Prevost) the mathematical formulation has been formulated in the Eulerian coordinate frame using the Jauman stress rate. However, these theories have a limitation of the applicability to soils by showing the oscillating behaviour at high strains as pointed out by Lee *et al.*,[31] Dafalias,[32] and Voyiadjis and Kattan.[33] Van der Berg[34] suggested the use of Arbitrary Lagrangian Eulerian (ALE) reference frame to improve this problem. Voyiadjis and Abu-Farsakh[21] adopted the updated Lagrangian coordinate frame to avoid this problem and to increase the accuracy of the solution.

The above-mentioned theories contributed a lot for the better understanding of the behaviour of the soils around the piezocone penetrometer. However, these methods (except Voyiadjis and Song[15]) did not predict the permeability of soils from the pore pressure response during PCPT 'on the fly'. The proposed method in this study, presented the 'on the fly' determination method of the permeability based on Voyiadjis and Abu-Farsakh's[21] coupled theory of mixtures, and completely removed the drawbacks of the conventional method.

## 3. PROPOSED METHOD

The proposed method is based on the idea that there is a clear relationship between the hydraulic properties of soil and the pore pressure difference between $u_2$ and $u_3$ locations. Elsworth[35–37] computed the hydraulic properties of soils with the linear elastic model using the dislocation method which is based on the work of Cleary.[38] From the view point of computational cost, the evaluation of the hydraulic properties using the linear elastic model is quite efficient. Considering that the strain is high at the vicinity of the cone tip (or porous tip), the linear elastic solution is not a very desirable solution. Ultimately, one should use the elasto-plastic large strain formulation. Voyiadjis and Song[15] computed the permeability of soils by directly correlating the permeability of the soils and the pore pressure at 'Real starting point of dissipation' in Figure 1. The application range of Voyiadjis and Song[15] is for the permeability $10^{-9}$ m/s–$10^{-6}$ m/s.

 

The main objective of this research is to develop a method for the determination of the permeability that can overcome the drawbacks of the conventional method and provide a more rational theoretical background or the broader range of permeability. The method proposed here utilizes the pore pressure generated during the PCPT and does not make use of the additional pore pressure dissipation data. This implies that this method utilizes the pore pressure at the 'Real starting point of dissipation' and 'Real dissipation curve' as shown in Figure 1. In utilizing the 'Real starting point of dissipation' and 'Real dissipation curve', the full interaction between the piezocone penetrometer and the soil is considered. Thus the problems discussed in Section 2 are completely eliminated.

To perform this approach, the formulation of the coupled field equations for soils using the theory of mixtures in an updated Lagrangian frame based on the principle of virtual work and implemented in a finite element program will be used. An axi-symmetric finite element program that is capable of describing the behaviour of soils with the advancement of the piezocone tips is coded. Finally, the validity of the proposed model is examined by comparing it with well-documented test results. The piezocone penetrometer penetrates into the ground with the speed of 2 cm/s, which induces the complete failure of soils around the cone tip. Recent research work[20,39–41] showed that the strain at the vicinity of the cone tip ranges between several tens percent to more than several hundreds percent. Thus penetration of the piezocone is essentially a time-dependent and large strain problem. To address this, the large strain, visco-plastic formulation must be incorporated for a reliable solution to this problem. Also, for the more general application of the model, the anisotropy of the soil must be also considered. However, in this study, visco-plasticity is not included. In this work, the simulation is conducted using the elastoplastic large strain approach with time-dependent loading condition. The modified Cam clay model is used in this study in order to describe the plastic behaviour of soils.

### *3.1. Basic concepts*

The proposed method utilizes the difference of pore water pressure at $u_2$ and $u_3$ locations. This method is valid only when there is a substantial difference between the pore pressure difference at $u_2$ and $u_3$ locations and the hydraulic properties. The test data and analytical results show that there is a clear difference between $u_2$ and $u_3$ locations. Whittle and Aubeny[42] showed analytically that there is a clear difference in pore pressure at $u_2$ and $u_3$ locations (See Figure 3). Robertson *et al.*[43] and Juran and Tumay[44] showed experimentally this behaviour.

Also, the typical data showed the clear difference in pore pressures at $u_2$ and $u_3$ locations (See Figure 4). Thus, undoubtedly one can see that there is a clear difference between the pore pressures at $u_2$ and $u_3$ locations. However, one can predict that the difference is very small for the fully undrained condition or the fully drained condition.

From Figure 5, one can expect that two values of the permeability are obtained from the one value of the pore pressure difference between the $u_2$ and $u_3$ locations. Thus, the direct relationship between the amount of pore pressure difference at $u_2$ and $u_3$ locations and the permeability may not be a reasonable way for the quantification.

A second method is utilizing the ratio of the pressure difference to the excess pore pressure at $u_2$ or $u_3$ locations by modelling the full length of penetration which is equal to the distance between $u_2$ and $u_3$. For real soils, this ratio will be small for low permeability and high for high permeability. This can be a better way for the quantification. However, this method requires the modelling of PCPT for 15 cm (approximate distance between $u_2$ and $u_3$ locations) penetration

 

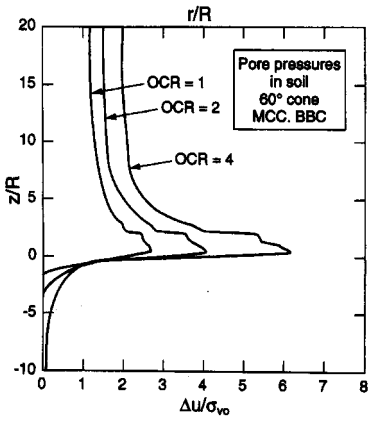


Figure 3. Excess pore pressure distribution around the cone tip (After Whittle and Aubeny,[42])

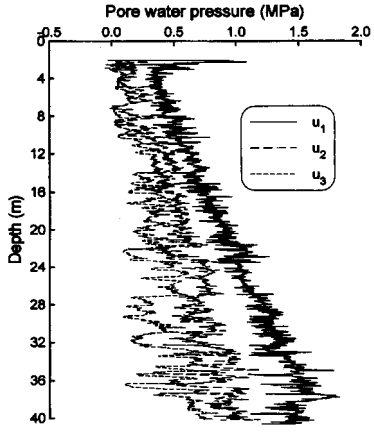


Figure 4. Field measured pore pressure from PCPT at Pentre, U.K. (After Powell and Quarterman,[45])

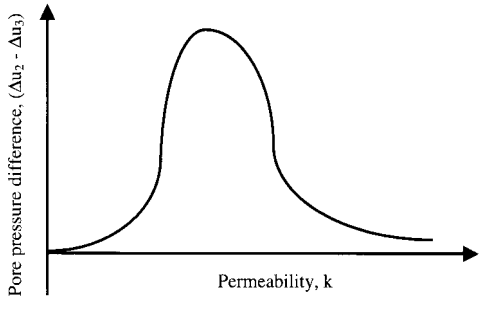


Figure 5. Conceptual relation between pore pressure difference and permeability

 

approximately. Modeling PCPT for 15 cm penetration for large strain incremental loading requires exhaustive computational effort, and is not feasible.

A third method is the consolidation approach. The pore pressure at $u_2$ and $u_3$ locations is different because of consolidation as well as the stress conditions. One can see the possibility that the pore pressure at the $u_3$ location is the dissipated pore pressure of the $u_2$ location. At the steady-state penetration one can reasonably assume that the shearing stress at $u_2$ and $u_3$ locations is identical. Then the pore pressure difference between $u_2$ and $u_3$ locations is due to the normal stress difference and pore pressure dissipation. Thus, if one can separate the shear stress-induced pore pressure and normal stress-induced pore pressure, one can compute the amount of the pore pressure dissipation between the $u_2$ and $u_3$ locations. This would lead to the permeability of the soil from the $u_2$ and $u_3$ that is directly measured during the PCPT. This concept is similar to the second method but it has great computational advantage.

Conclusively, the basic idea is that the pore pressure distribution at $u_2$ and $u_3$ represents the dissipation curve of the normal stress-induced excess pore pressure. Thus, starting the virtual consolidation at $u_2$ location for the normal stress-induced pore pressure with the assumed permeability; one can obtain the pore pressure at $u_3$ location. For the consolidation, $u_2$ is not taken as the initial pore pressure. The simultaneous generation and dissipation for the pore water is taken into account from the beginning of the PCPT throughout the virtual consolidation. Thus, the implicit drawbacks of the conventional method are inherently removed as well as the explicit drawbacks.

### *3.2. Theory of mixtures*

Soil consists of an assemblage of particles with different sizes and shapes, which forms a skeleton of which voids are filled with water and air or gas. The word 'soil', therefore, implies a mixture of assorted mineral grains with various fluids. Hence, soil in general must be looked at as a multiphase material whose state is to be described by the stresses and displacements (velocities) within each phase. The stresses carried by the soil skeleton are conventionally termed 'Effective stresses' in the soil mechanics literature,[17] and those by the water are called the 'pore water pressures'. When free drainage conditions prevail, the steady-state pore-water pressure depends only on the hydraulic conditions and is independent of the soil skeleton response to external loads. Therefore, in that case, a single phase continuum description of the soil behaviour is certainly adequate. Similarly, a single phase description of the soil behaviour is also adequate when no drainage (i.e. no flow) conditions prevail. However, in intermediate cases in which some flow can take place, there is an interaction between the skeleton strains and the pore water flow. The solution of these problems requires that the soil behaviour be analysed by incorporating the effect of the transient flow of the pore-water through the voids, and, therefore, requires that a multiphase continuum formulation be used for porous media. Biot[46,47] first developed such a theory for an elastic porous medium. However, it is observed experimentally that the stress–strain–strength behaviour of the soil skeleton is strongly non-linear, anisotropic, and elastoplatic. An extension of Biot's theory into the non-linear, anisotropic range is, therefore, necessary in order to analyse the transient response of soil deposits. This extension has acquired considerable importance in recent years due to the increased concern with the dynamic behaviour of saturated soil deposits and associated liquefaction of saturated sand deposits under seismic loading conditions. Such an extension of Biot's formulation is proposed by Prevost.[27,28]

 

In this work, Prevost's[27] theory of mixtures is coupled with Terzaghi's[17] effective stress theory as shown by Kiousis *et al.*,[48] Voyiadjis and Abu-Farsakh[21] and Abu-Farsakh *et al.*[30]. Thus a complete coupled theory of mixtures is obtained. The details of the coupled theory of mixtures are discussed in Section 3.3.

### *3.3 Formulation of the coupled theory of mixtures*

As discussed previously, the drainage condition around the penetrating cone tip is somewhere between the fully drained and the fully undrained condition. This condition is called the partially drained condition or the transient flow condition. For the transient flow condition it can be presumed that the pore pressure is a function of the permeability and other parameters.

Voyiadjis and Abu-Farsakh,[21] implemented the coupled theory of soil–water mixtures to the incremental large strain elastoplastic constitutive model, and derived the coupled equations. Here, similar equations are derived in a more refined manner.

From the principle of virtual work in an updated Lagrangian reference frame,[49] equation (2) is obtained:

$$ {}^{n+1}R = \int_{nV} {}^{n+1}_{n}S_{AB}\delta({}^{n+1}_{n}\varepsilon_{AB})\,\mathrm{d}^{n}V \tag{2} $$

In equation (2), ${}^{n}V$ is the volume of the element at the $n^{\text{th}}$ configuration, ${}^{n+1}_{n}S_{AB}$ is the second Piola–Kirchoff stress from $n^{\text{th}}$ to $(n+1)^{\text{th}}$ configuration, $\delta$ is the Kronecker delta, ${}^{n+1}_{n}\varepsilon_{AB}$ is the Green–Lagrangian strain from $n^{\text{th}}$ to $(n+1)^{\text{th}}$ configuration and ${}^{n+1}R$ is the external force at the $(n+1)^{\text{th}}$ configuration. Equation (2) can be rearranged as follows:

$$ \begin{aligned} {}^{n+1}R &= \int_{nV} ({}^{n}\sigma_{AB} + \Delta_{n}S_{AB})\delta({}^{n}e_{AB} + {}^{n}\eta_{AB})\,\mathrm{d}^{n}V \\ &= \int_{nV} ({}^{n}\sigma_{AB}\delta({}^{n}e_{AB} + {}^{n}\eta_{AB})\,\mathrm{d}^{n}V + \int_{nV} \Delta_{n}S_{AB)}\delta({}^{n}e_{AB} + {}^{n}\eta_{AB})\,\mathrm{d}^{n}V \end{aligned} \tag{3} $$

In equation (3), $\Delta_{n}S_{AB}$ is the increment of the second Piola–Kirchoff stress at the $n^{\text{th}}$ configuration. ${}^{n}e_{AB}$ is the linear strain at the $n$th configuration, and ${}^{n}\eta_{AB}$ is the non-linear strain at the $n^{\text{th}}$ configuration. In equation (3), $\Delta_{n}S_{AB}$ can be expressed as follows:

$$ \Delta_{n}S_{AB} = \int_{t}^{t+\Delta t} \dot{S}_{AB}\,\mathrm{d}t \tag{4} $$

From Abu–Farsakh and Voyiadjis,[29] $\dot{S}_{AB}$ can be expressed as follows considering the effective stress and the pore water pressure:

$$ \dot{S}_{AB} = D^{*}_{ABCD}\dot{\varepsilon}_{CD} + J^{s}X^{s}_{A,a}X^{s}_{B,b}\dot{P}_{w}\delta_{ab} \tag{5} $$

where,

$$ D^{*}_{ABCD} = [D_{abcd} - \sigma'^{s}_{cb}\delta_{ad} - \sigma'^{s}_{ac}\delta_{bd} + \sigma'^{s}_{ab}\delta_{cd} + P_{w}\delta_{ab}\delta_{cd} - 2P_{w}\delta_{ac}\delta_{bd}]J^{s}X^{s}_{A,a}X^{s}_{B,b}X^{s}_{C,c}X^{s}_{D,d} \tag{6} $$

 

In equations (5) and (6), $D^{*}_{\mathrm{ABCD}}$ is the modified elasto plastic modulus, $X^{\mathrm{s}}_{\mathrm{A,a}} = \partial^{n+1} X_{\mathrm{A}} / \partial^{n} X^{\mathrm{s}}_{\mathrm{a}}$, $\dot{\varepsilon}_{\mathrm{CD}}$ is the strain rate, $P_{\mathrm{w}}$ is the pore water pressure, $D_{\mathrm{abcd}}$ is the elastoplastic modulus, and $J$ is the Jacobian. Substituting $\dot{S}_{\mathrm{AB}}$ into equation (4), and making use of equation (6), one obtains:

$$\begin{aligned}
&\int_{nV} D^{*}_{\mathrm{ABCD}}(\Delta_n e_{\mathrm{CD}} + \Delta_n \eta_{\mathrm{CD}})\delta_n e_{\mathrm{AB}}\,\mathrm{d}^n V \\
&\quad + \int_{nV} D^{*}_{\mathrm{ABCD}}\Delta_n e_{\mathrm{CD}}\delta_n \eta_{\mathrm{AB}}\,\mathrm{d}^n V \\
&\quad + \int_{nV} ({}^{n}\sigma'^{\mathrm{s}}_{\mathrm{AB}} + {}^{n}P_{\mathrm{w}}\delta_{\mathrm{AB}})\delta_n \eta_{\mathrm{AB}}\,\mathrm{d}^n V \\
&\quad + \int_{nV} J^{\mathrm{s}} X^{\mathrm{s}}_{\mathrm{A,a}} X_{\mathrm{B,b}}\delta_{\mathrm{ab}}\Delta P\mathrm{w}(\delta_n e_{\mathrm{AB}} + \delta_n \eta_{\mathrm{AB}})\,\mathrm{d}^n V \\
&\quad = {}^{n+1}R - \int_{nV} ({}^{n}\sigma'^{\mathrm{s}}_{\mathrm{AB}} + {}^{n}P_{\mathrm{w}}\delta_{\mathrm{AB}})\delta_n e_{\mathrm{AB}}\,\mathrm{d}^n V
\end{aligned} \tag{7}$$

Equation (7) is the equation of equilibrium of the external and internal forces in an updated Lagrangian reference frame expressed in terms of the effective stress and pore water pressure. So far, the relationship between the pore water pressure and the permeability is not shown. This relationship can be derived from Prevost[27] such that:

$$-\operatorname{div}[(n^{\mathrm{w}}/\rho^{\mathrm{w}})\mathbf{K}^{\mathrm{ws}}(\operatorname{grad} P_{\mathrm{w}} - \rho_{\mathrm{w}}\mathbf{b} + \rho_{\mathrm{w}}\mathbf{a}^{\mathrm{w}})] + \operatorname{div}\mathbf{v}^{\mathrm{s}} = 0 \tag{8}$$

In equation (8), $\rho^{\mathrm{s}}$ is the mass density of the soil, $\rho^{\mathrm{w}}$ is the mass density of the water, $\mathbf{a}^{\mathrm{w}}$ is the acceleration of water, $\mathbf{K}^{\mathrm{ws}}$ is the permeability tensor, $\rho_{\mathrm{w}}$ is the density of water, $\mathbf{v}^{\mathrm{s}}$ is the solid velocity, $P_{\mathrm{w}}$ is the pore water pressure, and $\mathbf{b}$ is the body force vector. In the case when the acceleration is negligible, equation (8) reduces to;

$$-\operatorname{div}[(n^{\mathrm{w}}/\rho^{\mathrm{w}})\mathbf{K}^{\mathrm{ws}}(\operatorname{grad} P_{\mathrm{w}} - \rho_{\mathrm{w}}\mathbf{b})] + \operatorname{div}\mathbf{v}^{\mathrm{s}} = 0 \tag{9}$$

For an upgraded Lagrangian reference frame, equation (9) can be expressed as follows:

$$J^{\mathrm{s}} C^{\mathrm{s}}_{ij}\dot{\varepsilon}_{ij} - J^{\mathrm{s}} C^{\mathrm{s}-1}_{ij} C^{\mathrm{s}-1}_{ij} X^{\mathrm{s}}_{\mathrm{D,a}}(\partial/\partial X_{\mathrm{D}}) \times [(n_{\mathrm{w}}/\rho_{\mathrm{w}})K^{\mathrm{ws}}_{\mathrm{AB}} X^{\mathrm{s}}_{\mathrm{a,A}}(\partial P_{\mathrm{w}}/\partial X_{\mathrm{B}} - \rho_{\mathrm{w}} B_{\mathrm{B}})] = 0 \tag{10}$$

In equation (10), $C^{\mathrm{s}}_{ij} = X^{\mathrm{S}}_{\mathrm{K},I} X^{\mathrm{S}}_{\mathrm{K},J}$, $\dot{\varepsilon}_{ij}$ is the strain rate tensor, $X^{\mathrm{s}}_{\mathrm{a,A}} = \partial^{n+1} X_{\mathrm{a}} / \partial^{n} X^{\mathrm{s}}_{\mathrm{A}}$, $B_{\mathrm{b}} = b_{\mathrm{b}} / X^{\mathrm{s}}_{\mathrm{b,B}}$, and $J$ is the Jacobian. Using equations (7) and (10), the coupling of the stress, deformation, pore water pressure, and permeability is obtained. Thus, by solving equation (7) and (10) for the virtual consolidation, one can compute the permeability of the soil.

### *3.4. Numerical simulation*

By rearranging equations (7) and (10), one can obtain the following simplified equations:

$${}_{n}K\Delta U + {}^{n}\Omega\Delta W = {}_{n}\Phi \tag{11}$$

$$-{}_{n}\Omega^{t}\Delta U + {}_{n}\Psi\delta t\Delta W = {}_{n}\Pi \tag{12}$$

 

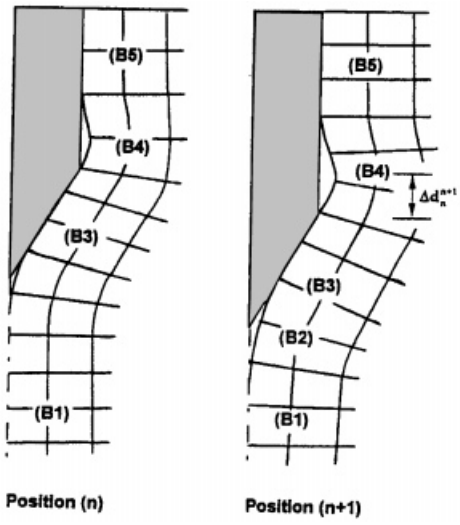


Figure 6. Incremental penetration of the piezocone (After Voyiadjis *et al.*[51])

In equations (11) and (12), ${}_nK$ is the stiffness matrix, ${}^n\Omega$ is the coupling matrix, ${}_n\Psi$ is the flow matrix, $\Delta U$ is the incremental nodal displacement, and $\Delta W$ is the incremental pore water pressure. Combining equations (11) and (12) in a matrix form, one obtains the following equations:

$$\begin{bmatrix} {}_nK & -{}_n\Omega \\ -{}_n\Omega^t & {}_n\Psi\delta t \end{bmatrix} \begin{bmatrix} \Delta U \\ \Delta W \end{bmatrix} = \begin{bmatrix} {}_n\Phi \\ {}_n\Pi \end{bmatrix} \tag{13}$$

The numerical simulation is conducted using an axi-symmetric finite element analysis. In this analysis, the piezocone penetrometer is assumed to be infinitely stiff and tensile stresses are not allowed to develop along the centreline boundaries. The continuous penetration of the piezocone is simulated by applying an incremental vertical displacement of the cone boundary as shown in Figure 6. The vertical displacement (penetration) is applied at the rate of two cm/s, at the same rate the miniature piezocone penetrates allowing for partial pore pressure dissipation during penetration. For numerical purposes, the piezocone penetrometer is assumed to be initially pre-bored to a minimum depth of 20 mm. This minimizes the error in assuming the initial stresses remain unchanged. A simple constraint approach at the nodal level, similar to the interface model proposed by Katona,[50] is adapted in this study to account for the soil-penetrometer interface friction. An angle of friction, $\delta = 14^\circ$, is assumed between the soil and the piezocone face. During the piezocone penetration, three interface states can be identified: fixed, slip and free states. Solution for the new nodal interface state is determined iteratively. Based on the previous interface state (fixed, slip or free) and the loading criterion, a new interface state is assumed and solved in order to obtain a trial solution. The trial solution is then used to check if the assumed trial state is correct. If not, a new state is assumed that is more likely to be correct.

At the beginning of penetration, all the nodes along the inclined conical surface and along the piezocone shaft are prevented from sliding along the surface and are forced to move vertically

 

Table I. Decision matrix for changing the boundary condition (After Voyiadjis et al.[51])

| Load step | $(k)$ 1 | 2 | 3 | 4 | 5 |
|---|---|---|---|---|---|
| $(k-1)$ | $F_n > 0$ & | $F_n < 0$ | $Y_n > Y_{tip}$ | | |
| 1 | $Y_n < Y_{tip}$ | (tension) | | | |
| 2 | $X_n < 0$ | $X_n > 0$ & $Y_n < Y_{tip}$ | $Y_n > Y_{tip}$ | | |
| 3 | | | $X_n < r_o$ | $X_n > r_o$ | |
| 4 | | | | $X_n > r_o$ | $X_n < r_o$ |
| 5 | | | | $F_n < 0$ | $F_n > 0$ |

with the cone boundary incremental movement until the sliding potential occurs. The sliding potential is reached when the tangent frictional force ($F_t$) of the node along the boundary surface reaches the allowable friction force ($F_t > F^s$) given by[51]

$$F^s = F_a^k + F_n^k \tan\delta \tag{14}$$

In equation (14), $F_a^k$ is the soil-piezocone adhesion force at the load increment $k$, $F_n^k$ is the normal effective force at the load increment $k$, and $\delta$ is the angle of friction between the soil and the piezocone surface. These nodes are afterwards allowed to slide along the skew boundary surface and along the cone shaft surface. During the incremental penetration, the nodes along the boundary are continuously checked for appropriate boundary condition adjustments. Based on the previous boundary conditions at load increment $(k-1)$, a new boundary condition state is assumed for the load increment $(k)$, depending on the load and displacement criteria. The validity of the assumed trial boundary condition is tested before one proceeds to the next loading increment. The decision matrix for selecting the new boundary condition is illustrated in Table I. If tension occurs ($F_n^k < 0$) in any of the nodes along the centreline boundary (B1 type) below the cone tip (Figure 6), the node is released and allowed to move freely and its boundary condition becomes a B2 type. The free nodes of type B2 are allowed to move freely until they reach the cone tip boundary ($Y_n > Y_{tip}$). These nodes are initially fixed and vertically displaced until the sliding potential is reached. After that they are allowed to slide along the skew conical surface and its boundary changes to B3 type. Once the horizontal coordinates of any node of type B3 boundary condition exceed the penetrometer radius ($X_n > r_o$), the node is then released and allowed to move freely and its boundary is changed to B4 type. Once the free nodes of B4 boundary return back to the penetrometer shaft boundary ($X_n < r_o$), they are then restricted from any further movement in the horizontal direction and allowed only to slide vertically along the cone shaft as indicated by B5 boundary type.

Numerical simulation was carried out for the miniature piezocone penetration tests (MPCPT) conducted at LSU/CALCHAS for the $K_o$-anisotropically consolidated specimen. The eight-node isoparametric finite element, Q8P4, is used in this analysis. The finite element mesh used in this analysis is presented in Figure 7.[21]

### *3.5. Formulation of the uncoupled consolidation*

For comparison with the result of coupled consolidation, approximate formulations for the uncoupled consolidation are derived. Using the notation of Figure 2, one can show that the

 

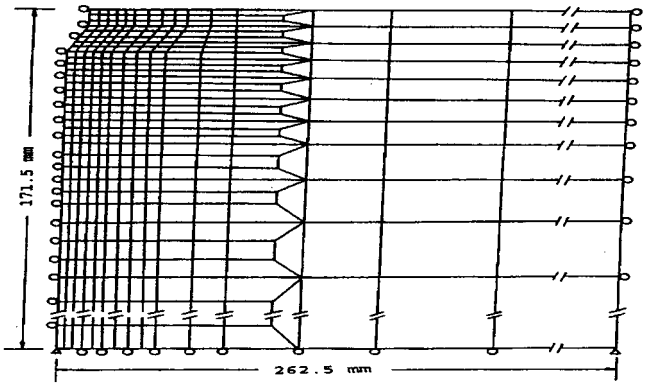


Figure 7. Finite element mesh for the piezocone penetration analysis. (After Voyiadjis and Abu–Farsakh.[21])

measured pore pressures at $u_2$ and $u_3$ locations are as follows:

$$u_2 = u_s + \Delta u_2 \tag{15}$$

$$u_3 = u_s + \Delta u_3 \tag{16}$$

In equations (15) and (16), $u_s$ is the hydro-static pressure, $\Delta u_2$ is the excess pore pressure at $u_2$ location, and $\Delta u_3$ is the excess pore pressure at $u_3$ location. The increment between $u_2$ and $u_3$ locations in equation (15) and (16) is expressed as equation (17):

$$u_2 - u_3 = (u_s + \Delta u_2) - (u_s + \Delta u_3) = (\Delta u_2 - \Delta u_3) \tag{17}$$

Also, noting that the excess pore pressure is the function of both the normal stress change and the shear stress change, one can obtain the following equation:

$$\begin{aligned} \Delta u &= \Delta u_n + \Delta u_s \\ &= \Delta u_{oct} + 3a\Delta\tau_{oct} \\ &= \Delta u_{oct} + 1{\cdot}4142\Delta\tau_{oct} \text{ (Assume } A = 1,\ a = (\sqrt{2}/3)\text{A)} \end{aligned} \tag{18}$$

In equation (18), $\Delta u_{oct}$ is the excess pore pressure induced by octahedral normal stress, $3a\Delta\tau_{oct}$ is the excess pore pressure induced by octahedral shear stress, '$a$' is Henkel's pore pressure coefficient, and '$A$' is Skempton's pore pressure coefficient.

Consequently equation (17) reduces to equation (19):

$$\Delta u_2 - \Delta u_3 = (\Delta u_{oct} + 1{\cdot}4142\Delta\tau_{oct})_2 - (\Delta u_{oct} + 1{\cdot}4142\Delta\tau_{oct})_3 \tag{19}$$

As mentioned previously, when one assumes that the shear stress at $u_2$ and $u_3$ location is identical, equation (19) becomes equation (20):

$$\Delta u_2 - \Delta u_3 = \Delta u_{oct,2} - \Delta u_{oct,3} \tag{20}$$

 

where, $\Delta u_{oct,2}$ is the octahedral normal stress-induced excess pore pressure at $u_2$ location and $\Delta u_{oct,3}$ is the octahedral normal stress-induced excess pore pressure at $u_3$. Also, one can see that $\Delta u_2$ is not $\Delta u_o$ because of the preceding dissipation; $\Delta u_2$ is smaller than $\Delta u_o$ in nature ($\Delta u_2 < \Delta u_o$). Thus, one can assume that $\Delta u_{o,normal} = \Delta u_o - 3a\Delta\tau_{oct} \Rightarrow \Delta u_{o,normal} < \Delta u_o \Rightarrow \Delta u_2 = \Delta u_{o,normal}$ (taking into account the preceding dissipation). Then the degree of consolidation can be calculated by

$$U = (\Delta u_o - \Delta u_t)/\Delta u_o = (\Delta u_2 - \Delta u_3)/\Delta u_{o,normal} \approx (\Delta u_2 - \Delta u_3)/\Delta u_2 \tag{21}$$

From Torstensson's[2,16] graphical solution, one can calculate the radial coefficient of consolidation $c_r$ or permeability $k$ ($k = c_r\gamma_w/M$, where $k$ is the permeability, $M$ is the constraint modulus, $\gamma_w$, is the unit weight of water) from $U$. Due to the inherent assumption of equation (21), the results are interpreted to have approximate values.

## 4. COMPARISION WITH TEST RESULTS

The collected field test results in Tables II and III are plotted in Figure 8 together with the theoretically predicted results. The collected field test results are for various soils. Thus a normalization of the field test results is performed for the reference undrained shear strength of 60 kPa. This normalization technique is based on the fact that the induced excess pore pressure is

Table II. Cases of the cone penetration-induced excess pore pressure and the permeability

| Site | Cohesion (kPa) | Permeability, $k$, (m/s) | Excess pore pressure, $\Delta u$ (kPa) | | Normalized excess pore pressure for cohesion = 60 kPa, $\Delta u$ (kPa) | | OCR | Reference |
|---|---|---|---|---|---|---|---|---|
| | | | $\Delta u_2$ | $\Delta u_3$ | $\Delta u_2$ | $\Delta u_3$ | | |
| Bakklandet Trondheim (Norway) | 100 | $1{\cdot}1 \times 10^{-9}$ | 550 | 250 | 330 | 150 | 1·7 | Sandven[53] |
| Pentre (U.K.) | 62·5 | $(2\text{–}8) \times 10^{-9}$ | 400 | 170 | 384 | 163 | 1·2–1·8 | Powell and Quarterman[46] |
| Bothkenner (U.K.) | 40–75 | $(1{\cdot}4\text{–}3) \times 10^{-9}$ | 500 | 340 | 400 | 272 | 1·0–1·5 | Lunne *et al.*[1] |
| Glava Stjørdal (Norway) | 90 | $6{\cdot}3 \times 10^{-10}$ | 600 | 420 | 400 | 280 | 3–4 | Sandven[53] |
| LSU Calibration Chamber | 60 | $7{\cdot}4 \times 10^{-9}$ | 330 | 200 | 330 | 200 | 1·5 | This study (K-33) |

Table III. Computational results

| Sites | Permeability, $k$ (m/s) | | |
|---|---|---|---|
| | Coupled consolidation | Uncoupled consolidation | Lab. test (vertical) |
| Bakklandet Trondheim (Norway) | $2 \times 10^{-8}$ | $2{\cdot}3 \times 10^{-8}$ | $0{\cdot}11 \times 10^{-8}$ |
| Pentre (U.K.) | $3 \times 10^{-8}$ | $1{\cdot}2 \times 10^{-8}$ | $(0{\cdot}2\text{–}0{\cdot}8) \times 10^{-8}$ |
| Bothkenner (U.K.) | $2 \times 10^{-8}$ | $6 \times 10^{-9}$ | $(1{\cdot}4\text{–}3) \times 10^{-9}$ |
| Glava Stjørdal (Norway) | $1{\cdot}5 \times 10^{-8}$ | $1{\cdot}5 \times 10^{-8}$ | $0{\cdot}063 \times 10^{-8}$ |
| LSU Calibration Chamber | $1{\cdot}3 \times 10^{-8}$ | $1{\cdot}7 \times 10^{-8}$ | $0{\cdot}74 \times 10^{-8}$ |

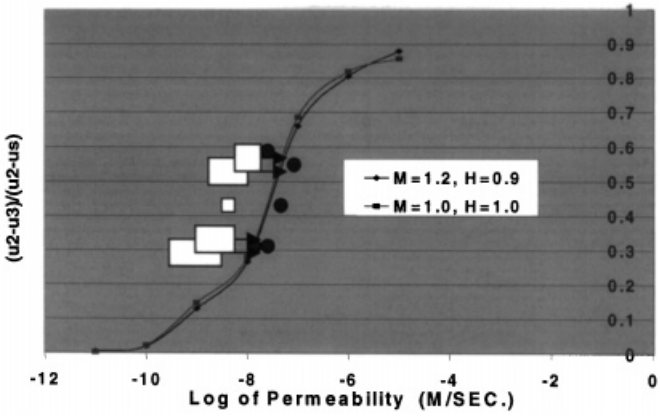


Figure 8. Change of pore pressure ratio $[(\Delta u_2 \_ \Delta u_3)/\Delta u_2]$ with permeability [ In the figure, $(u2 - u3)/(u2 - us)$ is the same as $(\Delta u_2 - \Delta u_3)/\Delta u_2$, rectangles represent the field test data of Table II, and solid dots represent the predicted values of permeability for the sites in Table II from the uncoupled consolidation]

proportional to the undrained shear strength as shown in equation (22) (Cavity Expansion theory, Vesic[52]).

$$\Delta u = s_u[0{\cdot}817\alpha_f + 2\ln(R_p/r)] \tag{22}$$

In equation (22) $s_u$ is the undrained shear strength, $\alpha_f$ is Henkel's pore pressure parameter, $R_p$ is the radius of the plastic zone, and $r$ is the distance to the center of cavity.

To evaluate the relationships between the PCPT-induced pore pressures and the permeability using the coupled theory of mixtures in an updated Lagrangian reference frame with an incremental elastoplastic constitutive model, the analyses are carried out utilizing the finite element program CS-S (Coupled System — Soils). This is performed for various permeabilities and strength parameters. In Figure 8, the parameter $(\Delta u_2 - \Delta u_3)/\Delta u_2$ (Note that both $\Delta u_2$ and $\Delta u_3$ are normalized.) is used as the reference parameter for the quantification of the relationship between the excess pore pressure and permeability. This parameter is used due to the fact that the direct increment of pore pressure $(\Delta u_2 - \Delta u_3)$ is not a function of a single permeability value as discussed in Figure 5.

In Figure 8, the two solid lines represent the change of $(\Delta u_2 - \Delta u_3)/\Delta u_2$ with permeability, $k$ for different values of $M$ and $H$, respectively (where, $M$ and $H$ are the properties of Cam-Clay model).

 

From the theoretically predicted lines in Figure 8, one can see that there is a clear relationship between the $(\Delta u_2 - \Delta u_3)/\Delta u_2$ and permeability in the permeability range from $10^{-10}$ to $10^{-6}$ m/s. The soil with permeability smaller than $10^{-10}$ m/s is a clayey soil with very low permeability and the soil with very low permeability and the soil with permeability higher than $10^{-6}$ m/s is a sandy soil with very high permeability.

Considering that the permeability criteria in general for the clay liners for sanitary land fill is $10^{-9}$ m/s and that for the free drainage materials for vertical drains and(or) horizontal drains is $10^{-5}$ m/s, the curves in Figure 8 show that there is a clear relationship between the parameter $(\Delta u_2 - \Delta u_3)/\Delta u_2$ and permeability for most of the field soils.

In Figure 8, the test results are indicated with rectangles instead of the points. The rectangles reflect the transient variational nature of the measured pore pressures during the PCPT as shown in Figure 4. The centre of the rectangles is the same as the values in Table II. In Table III, $\Delta u_2$ and $\Delta u_3$ values are taken from the mean $\Delta u_2$ and $\Delta u_3$ of the field measured pore pressure values.

It seems that the agreement between the test results and the theoretically predicted results is not quite good. However, since the representative field permeability values are typically much larger than the laboratory obtained values as reported by Baligh and Levadoux,[54] Song *et al.*[55] and Funeki,[56] therefore the rectangles of the test results in Figure 8 should move to the right. Then one can obtain an excellent agreement between the two. The arrows in Figure 8 represent this tendency. Thus, one can see the reasonable agreement between the predicted and the measured permeability values.

The solid and thick dots in Figure 8 represent the results from the uncoupled consolidation. The results from the uncoupled consolidation show a remarkably good agreement with the results obtained from the coupled consolidation. Considering its computational simplicity and implicit assumptions, these results are unexpected. Thus, one can see that the uncoupled consolidation method is also a good tool for the prediction of the hydraulic conductivity from the PCPT for the given soil condition in this study. However, considering that the uncoupled consolidation theory does not take into account the pore pressure interactions around the cone penetrometer, the results of the uncoupled consolidation may deviate substantially in certain conditions, thus its usage should be limited for the initial approximation only.

Also, Figure 8 shows that the relation between the pore pressure ratio $(\Delta u_2 - \Delta u_3)/\Delta u_2$ and permeability is not clear for the zones where the permeability is higher than $10^{-6}$ m/s or lower than $10^{-10}$ m/s. However, the meaning of permeability for these soils is not really significant in most of the civil engineering structures. However, the possibility of obtaining the permeability of these soils is shown in Table IV. Table IV shows the finite element analysis predicted excess pore pressures between $\Delta u_2$ and $\Delta u_3$ when $\Delta u_3$ is measured 80 s after measuring $\Delta u_2$. Eighty seconds means that the distance between $u_2$ and $u_3$ is 160 cm for the typical regular size cone (10 $cm^2$ cross section).

This distance is not practically feasible for the typical regular size cone. However, for the miniature cone, which has smaller cross section (assume 1 $cm^2$), the equivalent distance is reduced to 16 cm. This calculation is based on the radial consolidation concept as shown in equation (1). From equation (1), one can expect the following relationship such as

$$t = (T_r r^2 / c_r) \tag{23}$$

In equation (23), $t$ is the required time for a certain degree of consolidation, $T_r$ is the time factor for a certain degree of consolidation, and the other variables are the same as those in equation (1). Thus, by reducing the cross section of the cone penetrometer or increasing the distance between

 

Table IV. $\Delta u_2$ and $\Delta u_3$ when $\Delta u_3$ is taken after enough time lag (80 s) for $M = 1{\cdot}2$ and $H = 0{\cdot}9$

| Permeability (m/s) | $\Delta u_2$ (kPa) | $\Delta u_3$ (kPa) |
|---|---|---|
| $10^{-11}$ | 431 | 425 |
| $10^{-10}$ | 428 | 383 |
| $10^{-9}$ | 403 | 253 |
| $10^{-8}$ | 278 | 78 |
| $10^{-7}$ | 112 | 8·2 |
| $10^{-6}$ | 20 | 0·8 |
| $10^{-5}$ | 2·5 | 0·1 |

$u_2$ and $u_3$, one can obtain the permeability of the soil which is lower than $10^{-10}$ m/s. Also, by increasing the cross section of the cone penetrometer or decreasing the distance between $u_2$ and $u_3$, one can obtain the permeability of the soil which is higher than $10^{-6}$ m/s.

The 'one point method' of Voyiadjis and Song[15] is applicable for soils with permeabilities in the range $10^{-9}$ to $10^{-6}$ m/s. Figure 6 shows a wider range of application by using the proposed approach presented here, especially for lower permeability values (hereafter, the method of Voyiadjis and Song[15] is called the one-point method, and the method in this study is called the two points method). The one-point method has its own advantages in that it can be used without the modification of the existing piezocone penetrometer which has a piezo-element at the $u_1$ position. However, the two points method has its advantage that it can be applied for a wider range of permeabilities. Thus, one can see these two methods are compensating each other's disadvantages and constitute a complete new method when used together.

Conclusively, the discussions in this study show the capability of the coupled theory of mixtures to predict the permeability of the soil utilizing the penetrating pore pressure from the PCPT. From this study, it is shown that the agreement with the test data is quite reasonable. Thus, one can see the possibility of obtaining the continuous permeability profile, which was never possible in the past. Also, with the incorporation of the high-speed processor, the continuous permeability profile can be obtained. Furthermore, the real time ('on the fly') continuous permeability profile is obtained with substantially reduced cost.

## 5. CONCLUSION

A new theoretical interpretation and experimental verification of the two points cone penetration-induced excess pore pressure is carried out in this study. The large strain coupled theory of mixtures formulation using an updated Lagrangian reference frame is adopted in this work. Using this theory and the numerical simulation, the multi (2) piezo-element cone penetration induced excess pore pressure is used to predict reliably the permeability of the soil.

From this study, the following conclusions could be made:

The theoretically predicted permeability from the two points method agrees reasonably well with the field test data. Therefore, the results of this two points method can be used for the interpretation of the continuous pore pressure measurements, and can present the continuous permeability profile of the soil under investigation. Using the combination of the high-speed processor, this method can be used for the real-time continuous profile of the permeability of the soil.

 

Two threshold permeabilities are obtained as $10^{-10}$ and $10^{-6}$ m/s, respectively, for the fully undrained drainage condition and the free drained condition. Beyond these threshold permeability, the difference of the pore pressure change ratio $[(\Delta u_2 - \Delta u_3)/\Delta u_2]$ is not sensitive to the change of the permeability. Thus, the applicability of this method is not plausible. However, these threshold permeabilities are for the typical regular size of the cone with 10 $cm^2$ cross section. By changing the cone diameter and the distance between $u_2$ and $u_3$ positions, the threshold permeability can be moved outward. This is one of the advantages of the two points method compared to the one point method.

The results from the uncoupled consolidation agree remarkably well with the coupled consolidation for the conditions used in this study. However, uncoupled consolidation do not take into account the pore pressure interaction, and the coupling of the solid and pore water. The results using the uncoupled formulation should be used for initial approximation only. This study is carried out for the normally consolidated or lightly over consolidated soils. Thus the future study for the over consolidated soils will widen the applicability of this method.

This method is theoretically sound, and experimentally verified. Using this method, the efficiency of the piezocone penetration test can be increased significantly while the operating cost can be reduced substantially.

## REFERENCES


1. T. Lunne, P. K. Robertson and J. J. M. Powell, *Cone Penetration Testing*, Blackie Academic & Professional, 1997, pp. 1–7, 172–190, 218–222.
2. B. A. Torstensson, 'Pore pressure sounding instrument'. *Proc. ASCE, Spec. Conf. on In situ Measurement of Soil Properties*, Vol. II, Raleigh, N.C., 1975, pp. 48–54.
3. A. E. Z. Wissa, R. R. Martin and J. E. Galanger, 'The piezometer probe'. *Proc. ASCE Spec. Conf. on In situ Measurement of Soil Properties*, Raleigh, N.C., 1975, pp. 536–545.
4. M. T. Tumay, Y. Acar and R. L. Boggess, 'Subsurface investigation with piezocone penetrometer'. *ASCE Special Publication on Cone Penetration Testing and Experience*, *ASCE*, 1981, pp. 325–342.
5. H. M. Zuidberg, L. H. J. Schaap and F. Beringen, 'A penetrometer for simultaneous measurement of cone resistance, sleeve friction and dynamic pore pressure'. *Proc. ESOPT II*, Amsterdam, Vol. 2, 1982, pp. 963–970.
6. M. M. Baligh, A. S. Azzouz, A. Z. E. Wissa, R. T. Martin and M. J. Morrison, 'The piezocone penetrometer'. *ASCE, GE. Div. Symp. on Cone Penetration Testing and Experience*, St. Louis, 1982, pp. 247–263.
7. R. G. Campanella and P. K. Robertson, 'Applied cone research'. *ASCE, GE Div. Symp. on Cone Penetration Testing and Experience*, St. Louis, 1981, pp. 343–362.
8. T. Muromachi, 'Cone penetration testing in Japan'. *ASCE, Geomech. Engng. Div. Symp. on Cone Penetration Testing and Experience*, St. Louis, 1981, pp. 76–107.
9. J. de Ruiter, 'The static cone penetration test: state–of–art report'. *Proc. Second European Symp. on Penetration Testing, ESOPT II*, Amsterdam, Vol. 2, 1982, pp. 389–405.
10. F. P. Smits, 'Penetration pore pressure measured with piezometer cones'. *Proc. ESOPT II*, Amsterdam, Vol. 2, 1982, pp. 877–881.
11. R. G. Campanella, Lecture Note, presented to Korean Geotechnical Society, 1994.
12. M. T. Tumay, P. Kurup and R. L. Boggess, 'A Continuous intrusion electronic miniature cone penetration tests systems for site characterization'. *Proc. Int. Conf. on Site Characterization, '98,* Atlanta, GA, April 19–22, Vol. 2, 1998, pp. 1183–1188.
13. Environmental Mechanics AB, Company Brochures. Sweden, 1997.
14. P. W. Mayne and G. J. Rix, 'Development of a Seismic Piezocone pressuremeter for evaluating the in situ $G/G_{max}$ degradation characteristics of soils'. GeoSystems web page, 1996.
15. G. Z. Voyiadjis and C. R. Song, 'Determination of the hydraulic conductivity of soils using continuous intrusion piezocone penetration test'. *J. comput. geotechn.* submitted for publication. 1998.
16. B. A. Torstensson, 'The pore pressure probe'. *Paper 34, Geotech. Meeting, Norwegian Geotech. Soc.*, Oslo, Norway. 1997, pp. 34.1–34.15.
17. K. Terzaghi, *Theoretical Soil Mechanics*, Wiley, New York, 1943, pp. 265–296.
18. R. C. Gupta and J. L. Davidson, 'Piezoprobe determination of the coefficient of consolidation'. *Soils Found.*, **26**(3), 12–22 (1986).


 

19. P. U. Kurup and M. T. Tumay, 'Piezocone dissipation curves with initial pore pressure variation'. *CPT'95*, *Proc. Int. Symp. on Cone Penetration Testing*, 1995, pp. 195–200.
20. P. U. Kurup and M. T. Tumay, 'A numerical model for the analysis of piezocone dissipation curves'. in Pieruszczak and Pande (eds.), *Numerical Models in Geomechanics*, Balkema, Rotterdam, 1997, pp. 353–358.
21. G. Z. Voyiadjis and Y. M. Abu–Farsakh, 'Coupled theory of mixtures for clayey soils'. *Compu. Geotech.* **20**(3–4), 195–222 (1997).
22. R. E. Gibson, G. L. England and M. J. L. Hussey, 'The theory of one–dimensional consolidation of saturated clays, I Finite non-linear consolidation of thin homogeneous layers'. *Geotechnique*, **17,** 261–273 (1967).
23. R. E. Gibson, R. L. Schiffman and K. W. Cargill, 'The theory of one–dimensional consolidation of saturated clays, II Finite non-linear consolidation of thick homogeneous layers'. *Canadian geotechn. J.* **18,** 280–293 (1981).
24. R. L. Schiffman, 'Finite and infinitesimal strain consolidation'. *J. Geomech Engng. Div. ASCE*, **106**(GT2), 203–207 (1980).
25. J. P. Carter, J. C. Small and J. R. Booker, 'A theory of finite elastic consolidation'. *J. Solids Struct*. **13,** 467–478 (977).
26. J. P. Carter, J. R. Booker and J. C. Small, 'The analysis of finite elastoplastic consolidation'. *Int. J. Num. Anal. Meth. Geomechan.* 561–565 (1979).
27. J. H. Prevost, 'Mechanics of continuous porous media'. *Int. J. Engng. Sci.* **18,** 787–800 (1980).
28. J. H. Prevost, 'Consolidation of an elastic porous media'. *J. Engng. Mech. Div. ASCE*, **107**(EM1), pp. 169–186 (1981).
29. M. Y. Abu–Farsakh, G. Z. Voyiadjis and M.T. Tumay, 'Numerical Analysis of the Miniature Piezocone Penetration Tests (PCPT) in cohesive soils', *Int. J. Numer. Anal. Meth. Geomechan.* **22,** 791–818 (1998).
30. P. D. Kiousis and G. Z. Voyiadjis, 'Lagrangian continuum theory for saturated porous media'. *J. Engng. Mech. ASCE*, **111**(10), pp. 1277–1288 (1985).
31. E. H. Lee, R. L. Mallett and T. B. Wertheimer, 'Stress analysis for anisotropic hardening in finite-deformation plasticity'. *Trans ASME, J. Appl. Mech.* **50,** 554–560 (1983).
32. Y. F. Dafalias, 'Corotational rates for kinematic hardening at large plastic deformations'. *Trans. ASME, J. Appl. Mech.* 561–565 (1983).
33. G. Z. Voyiadjis and P. I. Kattan, 'Eulerian constitutive model for finite deformation plasticity with anisotropic hardening'. *Mech. Mater.* **7**(4), 279–293 (1989).
34. P. van der Berg, 'Cone penetration in layered media, an ALE finite element formulation'. *XIII J. ICSMFE*, 1957–1962 (1993).
35. D. Elsworth, 'Analysis of piezocone dissipation data using dislocation methods'. *J. Geomech Engng. ASCE*, **119**(10), pp. 1601–1623 (1993).
36. D. Elsworth, 'Dislocation analysis of penetration in saturated porous media'. *J. Engng. Mech. ASCE*. **117**(2), pp. 391–408 (1991).
37. D. Elsworth, 'Pore–pressure response due to penetration through layered media'. *Int. J. Numer. Anal. Meth. Geomechan.* **16,** pp. 45–64 (1992).
38. M. P. Cleary, 'Fundamental Solutions for a fluid–saturated porous solid'. *Int. J. Solid Struct*., **13,** 785–806 (1977).
39. M. T. Tumay, Y. B. Acar, M. H. Cekirge and N. Ramesh, 'Flow field around cones in steady penetration'. *J. Geomech Engng. Div. ASCE*, **111**(2), 193–205 (1985).
40. J. N. Levadoux and M. M. Baligh, 'Consolidation after undrained piezocone penetrometer, I: prediction'. *J. Geomech. ASCE*, **112**(7), 707–725 (1986).
41. P. D. Kiousis, G. Z. Voyiadjis and M. T. Tumay, 'A large strain theory for the two dimensional problems in geomechanics'. *Int. J. Numer. Anal. Meth. Geotech.* **10,** 17–39 (1986).
42. A. J. Whitle and C. P. Aubeny, 'Pore pressure fields around piezocone penetrometers installed in clay'. *Proc. 7th Int. Conf. on Computer Methods and Advances in Geomechanics*, Cairns, 1, Balkema, Rotterdam, 1991, pp. 285–290.
43. P. K. Robertson, R. G. Campanella, D. Gillespie and J. Greig, 'Use of piezometer cone data'. *Proc. ASCE Specialty Conf. on in situ*'86: *Use of In Situ Tests in Geotechnical Engineering*, Blacksburg, 1986, pp. 1263–1280.
44. I. Juran and M. T. Tumay, 'Soil stratification using dual pore–pressure piezoconetest, DPCPT', *Transportation Research Board Record, No*, 1235, Transportation Research Board, National Research Council, May. 1990, pp. 68–78.
45. J. J. M. Powell and R. S. T. Quarterman, 'A study of piezocone dissipation tests in soft clays for consolidation properties', (excepted from Lunne, Robertson, Powell (1997)), 1997, in preparation.
46. M. A. Biot, 'New concepts and methods', *Q. Appl. Math.* **36,** 19 (1978).
47. M. A. Biot, 'Theory of Elasticity and Consolidation for a Porous Anisotropic Solid', *J. Appl. Phys.* **26,** 182–185 (1955).
48. P. D. Kiousis, G. Z. Voyiadjis and M. T. Tumay, 'A large strain theory and its application in the analysis of the cone penetration mechanism', *Int. J. Numer. Anal. Meth. Geomechan.* **12**(1), 45–60 (1988).
49. K. J. Bathe, *Finite Element Procedures*, Prentice Hall, Engle wood Cliffs, NJ, 1996, 485–641.
50. M. G. Katona, 'A simple contact–friction interface element with applications to buried culvert', *Int. J. Numer. Anal. Meth. Geomechan.* **7,** 371–384 (1983).
51. G. Z. Voyiadjis, M. Y. Abu–Farsakh and M. T. Tumay, 'Soil deformations around the piezocone using the coupled theory of mixtures', *Poromechanics a Tribute to Maurice A. Biot*, *Proc. Biot Conf. on Poromechanics*, Louvain–Neuve/Belgium/14–16, September, 1998, pp. 531–536.

 

52. A. S. Vesic, 'Expansion of cavities in infinite soil mass', *J. Soil Mechan. Foundation Div. ASCE*, **98,** 265–290 (1972).
53. R. Sandven, 'Strength and deformation properties of fine grained soils obtained from piezocone tests', *Ph. D Dissertation*, Institute for Geoteknikk, Trondheim, Norway, 1990.
54. M. M. Baligh and J. N. Levadoux, 'Consolidation after undrained piezocone penetration, Part II: Interpretation', *J. Geomech. Engng. Div. ASCE*, **112**(7), pp. 727–745 (1986).
55. C. R. Song, D. Y. Oh, S. S. Kim and B. S. Chun, 'Consolidation characteristic by field monitoring', *Proc.* 1*st Int. Conf. on Soft Soil Engineering*, 1993, pp. 584–589.
56. Funeki, 'Time dependent settlement behavior of soft soil under loading (with emphasis on settlement prediction method)', *Ph. D. Dissertation*, Kyoto Univ. 1976, pp. 226–229 (in Japanese).

 